Research Article

Fatin Nur Amirah Mohd Sabri, Muhammad Razlan Zakaria, Hazizan Md Akil*, Mohd Shukur Zainol Abidin, Aslina Anjang Ab Rahman, and Mohd Firdaus Omar

Interlaminar fracture toughness properties of hybrid glass fiber-reinforced composite interlayered with carbon nanotube using electrospray deposition

https://doi.org/10.1515/ntrev-2021-0103
received May 11, 2021; accepted September 20, 2021

Abstract: The electrospray deposition (ESD) method was used to deposit carbon nanotubes (CNTs) onto the surface of glass fiber (GF). The morphology of the hybrid CNTs-GF was analyzed using a field emission scanning electron microscope, and the images indicated that the CNTs were uniformly and homogenously deposited onto the GF's surface. Laminated composite based on GF and hybrid CNTs-GF were then fabricated *via* vacuum-assisted resin transfer molding. The mode I interlaminar fracture toughness was measured using the double cantilever beam test method. The hybrid CNTs-GF showed a 34% increase in fracture toughness relative to the control sample. The mechanism of interlaminar fracture toughness enhancement was elucidated *via* fractography, where fiber bridging, adhesive and cohesive failures, hackles, and coarse matrix surface were observed along the crack pathways.

Keywords: glass fiber, carbon nanotubes, electrospray, interlaminar fracture toughness

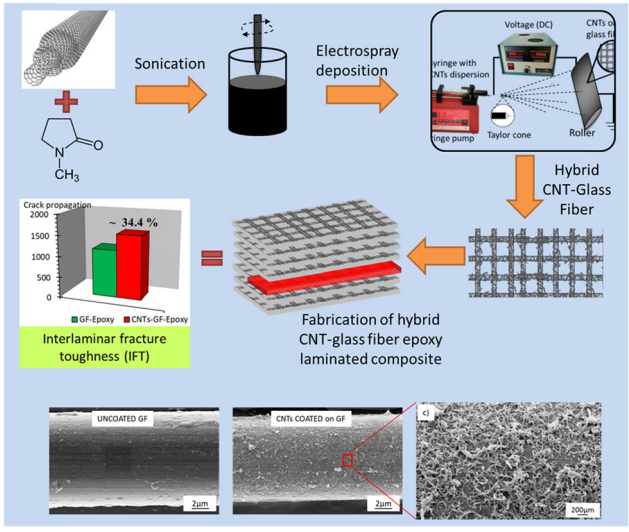

Graphical abstract

1 Introduction

Fiber-reinforced polymer (FRP) is fast becoming one of the essential materials in engineering and is widely used in aerospace applications, sporting goods, automobiles, and civil and marine structures [1]. The FRP system is a system where embedded fibers, such as glass or carbon, serve as reinforcements within a polymer matrix [2]. They are well-known for their high strength-to-weight ratio, excellent corrosion resistance, in-plane strength-to-weight ratio, and fatigue resistance [3,4]. Although FRP has excellent in-plane strength, it has poor strength in the thickness direction due to its lack of fiber reinforcement to support loads in the transverse direction [5], making woven fabric-laminated composites susceptible to delamination failure, which substantially decreases its subsequent strength and stiffness [6].

Delamination is a failure mode often encountered in laminated composite systems, where the layers are

* **Corresponding author: Hazizan Md Akil,** School of Materials and Mineral Resources Engineering, Engineering Campus, Universiti Sains Malaysia, 14300 Nibong Tebal, Pulau Pinang, Malaysia, e-mail: hazizan@usm.my
Fatin Nur Amirah Mohd Sabri: School of Materials and Mineral Resources Engineering, Engineering Campus, Universiti Sains Malaysia, 14300 Nibong Tebal, Pulau Pinang, Malaysia
Muhammad Razlan Zakaria, Mohd Shukur Zainol Abidin, Aslina Anjang Ab Rahman: School of Aerospace Engineering, Engineering Campus, Universiti Sains Malaysia, 14300 Nibong Tebal, Pulau Pinang, Malaysia
Mohd Firdaus Omar: Faculty of Chemical Engineering Technology, Universiti Malaysia Perlis (UniMAP), Perlis, Malaysia

separated from one another [7]. Poor interfacial adhesion is a major factor causing delamination failure [8,9]. Delamination in woven fabric-laminated composite causes failures such as the bridging phenomenon, fiber failure, fiber pull-out, matrix plastic deformation, and delamination front deflection [10]. Besides, the crack growth behavior of woven laminated composite exhibits intrinsically unstable crack growth relative to the unidirectional laminated composites due to the characteristics of neighboring plies (longitudinal and transversal tows) where the crack jumps between the transverse tows. The presence of inclusions and resin-rich area in the weave structure serves as one of the toughening mechanism in woven fabric-laminated composite [3]. To address these issues, previous researchers had introduced the filler such as carbon nanotubes (CNTs) or graphene as nano-phase reinforcement.

Enhancement of interlaminar fracture toughness of laminated composite is influenced by factors such as Z-pining, 3D weaving, fiber hybridization, short fiber, and toughening of the matrix resin [11]. The introduction of nano-phase reinforcements such as CNTs into the interlaminar region of the laminated composites can be regarded as a promising method toward improving interlaminar fracture toughness due to the extraordinary properties of CNTs such as high stiffness and strength, specific surface area, and aspect ratios [12–14]. The presence of CNTs also provides additional toughening mechanism against fiber pull-out, CNT peeling, hackles formation, and stick-slim formation [15].

The CNTs can be introduced into laminated composites by directly embedding it into the polymer matrix [16,17], but this approach faces difficulties in achieving homogenous dispersion of the CNTs due to the strong Van der Walls forces, leading to agglomeration [18,19]. Also, the high viscosity of the CNTs dispersion in the resin makes the process complicated, which leads to poor efficiency performance in the laminated composites [20]. To address the CNTs agglomeration problem, the CNTs can be directly grown or deposited onto the fiber surface.

Few methods that successfully grew or deposited CNT onto fiber surfaces have been reported, such as chemical vapor deposition (CVD), electrophoretic deposition (EPD), chemical grafting, traditional spray-up, and electrospray deposition (ESD), each with its respective advantages and limitations [21]. For example, the high processing temperature in the CVD method compromises the fiber properties and burns off the sizing of fiber coating [22]. Low-temperature methods such as EPD, chemical grafting, and traditional spray-up are viable replacements for the high-temperature approach [23]. However, excessive exposure of the fiber to chemicals and the required oxidation treatment could structurally damage the CNTs and fibers [24]. Traditional spray-up approach encountered difficulties in dispersing CNT homogenously due to its large droplet size [25]. As compared to other methods, the ESD method can overcome the limitation by deposition of the CNTs on the fiber surface with the applied voltage. ESD is a simplified method that can be conducted at room temperature and does not require any oxidation treatment for the fibers. It uses a high electrical field that converts the suspension of CNTs into non-agglomerating uniform-sized nanodroplets to be deposited onto the target. As reported by Li *et al.* [26], the ESD method successfully produced a homogeneous and well-distributed coating of CNTs into fibers, while maintaining mechanical performance. This is due to the use of high electrical field, which converts the suspension of CNTs into uniformly sized nano or microdroplets in the target. In addition to being a simpler method, ESD provided cost effectiveness, versatility, and large-scale production.

This study intends to address issues involving the deposition of CNTs onto fiber surfaces using the ESD method, while also improving the fracture toughness of the final product. The hybrid CNT-glass fiber (GF) was prepared, and the effectiveness of the hybrid GF interlayered with CNT by the ESD method was analyzed. The surface morphology hybrid of the CNT-GF was characterized using a field emission scanning electron microscope (FESEM). Then, the hybrid CNT-GF-Epoxy-laminated composite was fabricated using the vacuum-assisted resin transfer molding (VARTM) method. The interlaminar fracture toughness was determined using the opening mode I test double cantilever beam (DCB). The aim of this study is to investigate the CNT deposited *via* the ESD method on the GF surface and evaluate its fracture toughness performance when used in a fabric-laminated composite system. The process is shown in graphical abstract.

2 Experimental method

2.1 Materials

Woven "E" GF (CL Composites Sdn. Bhd) with a density of 2.56 g cm^{-3} and area weight of 400 g m^{-2} were used in this study. The multiwalled CNTs were purchased from Skyspring Nanomaterials, Inc, Houston, TX, USA, with purity of 95%, an external diameter of ~20–30 nm, and

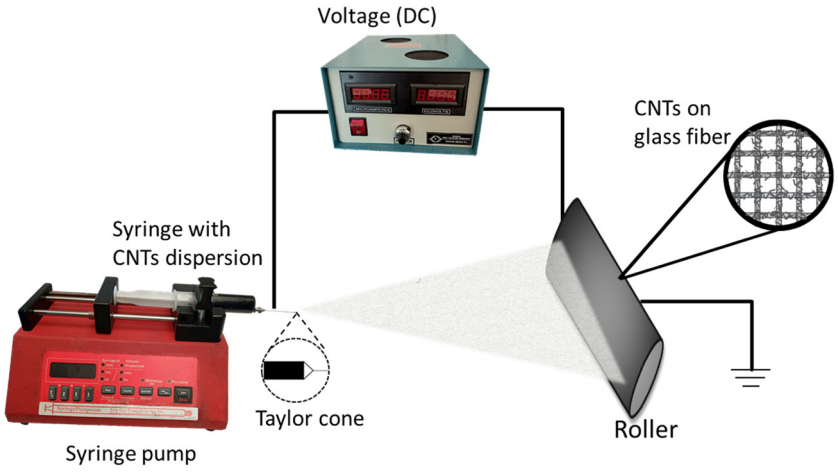

Figure 1: Illustration of ESD process.

internal diameter of ~10–30 µm. Merck supplied the *N*-methyl-2-pyrrolidone (NMP) solvent. The epoxy resin used in this work was of the EpoxAmite® 100 part, a variety with hardener EpoxAmite® 103 slow part B supplied by Smooth-On Inc. This epoxy system was preferred due to its low viscosity and slow curing, making it suitable for the VARTM process.

2.2 Preparation of CNTs-deposited GF

The hybrid CNTs-GF was prepared using the ESD technique. First, the dispersion of CNTs was prepared by dispersing 0.1 g of CNTs into 50 mL of NMP. The dispersion was sonicated for 8 h using a probe ultrasonicator at 40 kHz to prevent CNTs agglomeration. The dispersion was then sprayed onto the both surfaces of the GF attached to the roller using a voltage of 18 kV for 15 min. The roller was rotated at a fixed speed of ~120 rpm and the dispersion flow rate was of 0.02 mL h^{-1} during the process. The entire process is shown in Figure 1. Note that the process parameters used in this study were the optimized conditions discovered in previous work that has been previously reported with slight modification in applied voltage and time of sonication [21,26,27].

2.3 Preparation of hybrid CNTs-GF epoxy laminated composite

The VARTM process was used to produce the laminate composites consisting of eight plies of hybrid CNTs-GF with a dimension of 210 mm × 297 mm, as shown in Figure 2 (a) upper mold and (b) lower mold. The mold was designed based on the perimeter-to-point model of the infusion technique. Epoxy-laminated composites were prepared using the 1:2 fiber-to-resin weight ratio. The EpoxAmite® 100 part A was mixed with the hardener EpoxAmite® 103 slow part B and then degassed at room temperature. Eight plies of hybrid CNTs-GF were stacked with PTFE film inserted in the middle of the plies as a crack starter, as

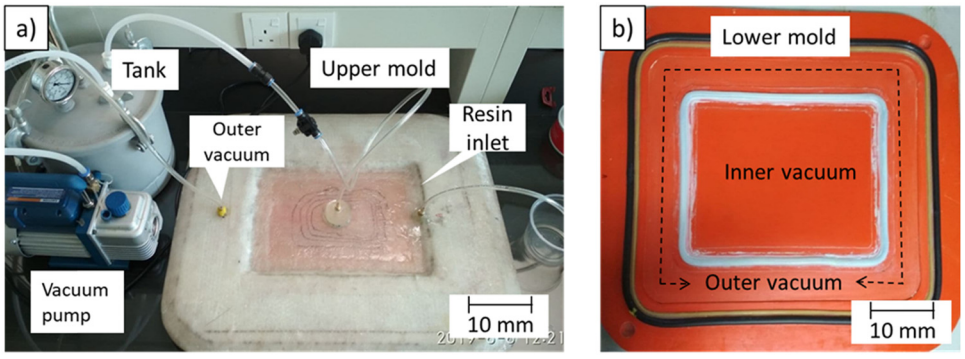

Figure 2: Experimental setup for VARTM process (a) upper mold and (b) lower mold.

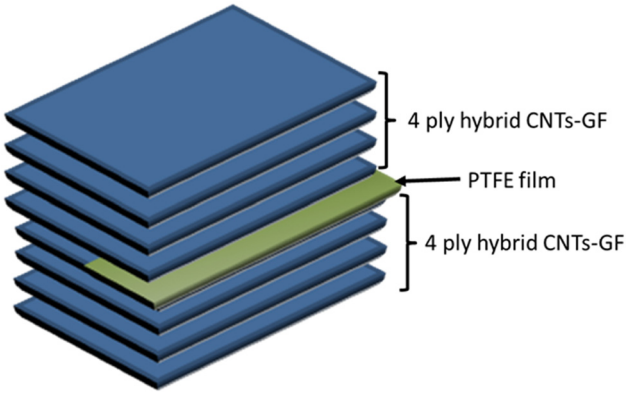

Figure 3: Illustration of sample preparation of hybrid CNTs-GF.

shown in Figure 3. A 13 µm-thick PTFE film with a length of 60 mm was used in this study. The mixture of epoxy resin was inserted into the mold *via* the resin inlet under a vacuum pressure of 75 cm Hg. The mixture flowed in the direction across the fiber layers until it reached the vent at the top of the mold. After infusion, all the inlet and outlet vacuum were shut to maintain constant pressure, then left overnight to cure at room temperature (25°C). The sample is described in Table 1.

2.4 Characterization of hybrid GF-CNTs-epoxy-laminated composite

The surface morphology of the CNTs deposited onto the surface of GF and the fracture samples of the DCB test were analyzed using the FESEM (FESEM, Zeiss Supra 35VP). The constituent volume fraction of each sample was measured as per the ASTM D 3171 procedure G, and the data were used in the formula below:

$$V_f = \left(\frac{M_f}{M_c}\right) \times 100 \times \left(\frac{P_c}{P_f}\right), \quad (1)$$

$$V_m = \left(\frac{M_m}{M_c}\right) \times 100 \times \left(\frac{P_c}{P_f}\right), \quad (2)$$

$$M_m = M_c - M_f, \quad (3)$$

where V_f is the fiber volume fraction, M_f is the mass of fiber after digestion, M_c is the mass of the initial composite, P_c is the density of the composite, P_f is the density of the fiber, V_m is the matrix volume form, M_m is the mass of the matrix after ignition, and P_m is the density of the matrix.

The DCB sample was prepared as per ASTM D5528, with loading blocks, as shown in Figure 4. The samples were with dimensions of 150, 25, and 3.5 mm. Two aluminum blocks were attached at the end of the sample with epoxy adhesive and cured overnight at room temperature. The crack length scale was drawn at the side of the sample to allow for the observation of the crack tip during delamination. Mode I: Interlaminar fracture toughness was investigated using the Testometric with a load cell of 50 kN. The test setup is shown in Figure 5. The samples were pre-cracked at a crosshead speed rate of 5 mm min^{-1} and then unloaded to the initial position. The test was resumed at a speed of 1 mm min^{-1} until it reached a crack length of 25 mm. A minimum of five samples of each category was tested, and the data were collected and analyzed based on the corrected beam theory (CBT).

$$G_{IC} = \frac{3P\delta}{2B(a + |\Delta|)}, \quad (4)$$

$$C = \frac{8\,(a + \Delta)^3}{E_f b h^3}, \quad (5)$$

$$C = \frac{\delta}{P}, \quad (6)$$

$$E_f = \frac{8}{m^3 b h^3}, \quad (7)$$

where P is the applied load, δ is the crosshead displacement, a is the crack length, C is the compliance, b is the sample's width, h is the arm thickness, Δ is the correction for beam rotation at the crack tip determined from the x-axis intercept of the $C^{1/3}$ against crack length plot, E_f is the flexural modulus of the arm, and m is the gradient.

3 Results and discussions

The surface morphologies of the woven GF before and after the deposition of CNTs are shown in Figure 6. Figure 6a shows the FESEM image of a woven GF before the CNTs deposition. The smooth surface of the GF is

Table 1: The samples description

	Control sample	Hybrid sample
Sample name	GF-Epoxy	CNTs-GF-Epoxy
Description	Epoxy reinforced with 8-plies of GF	Epoxy reinforced with 8-plies of deposited CNTs on GF

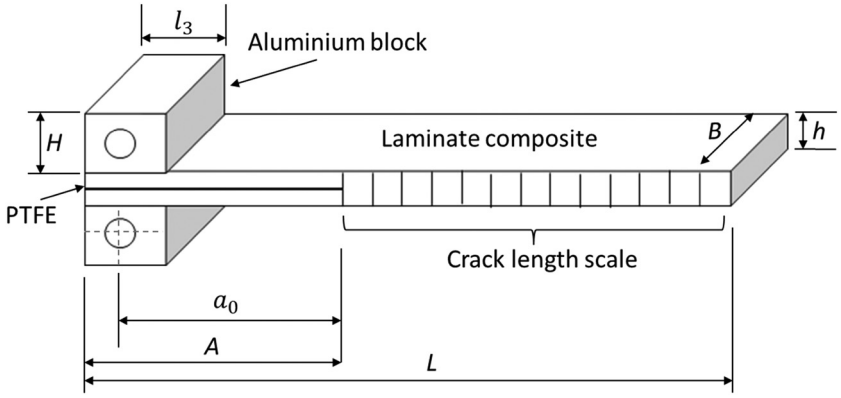

Figure 4: The sample dimension for DCB test.

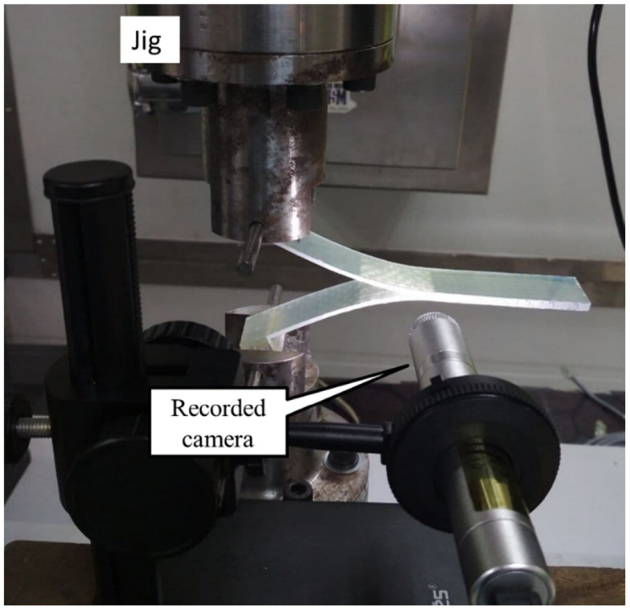

Figure 5: Experimental setup for DCB test.

evident in the image. The morphology of the hybrid CNTs-GF after deposition is shown in Figure 6b and c. Homogenous and uniform deposition of CNTs on the surface of GF was successfully done, as per Figure 6b. Based on the observed morphologies, it can be surmised that the ESD method successfully deposited CNTs onto the GF surface, at minimal agglomeration.

The constituent of volume fraction for each sample is detailed in Table 2. The results show both samples having fiber volume fractions of ~29–32% and matrix volume fractions of ~67–70%.

The load-opening displacement curves representing Mode I from the DCB test for the control sample (GF-Epoxy) and hybrid sample (CNTs-GF-Epoxy) are shown in Figure 7. The fracture toughness was evaluated at the initiation (pre-cracked) and propagation (crack propagation) stages. The curve shows the crack front progressed 25 mm from its pre-crack stage. The *R*-curve in Figure 7 represents the sample's crack growth resistance. The hybrid sample (CNTs-GF-Epoxy) exhibited a relatively longer displacement and higher load for growing the same crack length relative to the control sample (GF-Epoxy) composite. The *R*-curve shows a relatively non-linear behavior, displaying a combination of stable and unstable crack growths where the load suddenly drops alongside the crack growth [3].

In a woven composite system, the propagation of a crack is determined by the weave's geometry. Thus, the fracture behavior relies on fiber architecture, resulting in

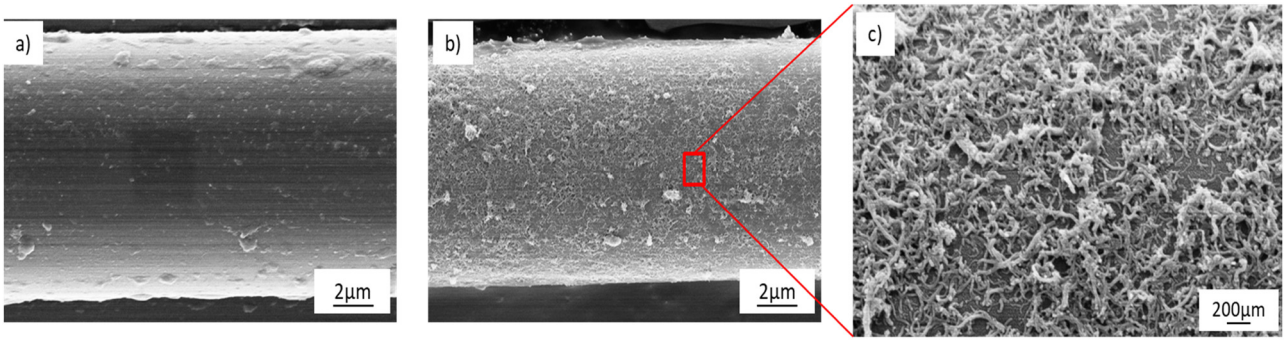

Figure 6: FESEM image of (a) GF, (b) and (c) hybrid CNTs-GF at 5k× and 20k× magnifications, respectively.

Table 2: The constituent of volume fraction of control and hybrid sample

	Fiber volume fraction, V_f (%)	Matrix volume fraction, V_m (%)
GF-Epoxy	29.93 ± 0.8	69.94 ± 0.8
CNTs-GF-Epoxy	32.35 ± 0.8	67.51 ± 0.7

less cracking of the matrix [28]. The neighboring 0°/90° interphase and transverse tows in the woven fiber produce crack jumping, which resulted in unstable crack growth. Each sample exhibits a sawtooth reaction, which is a feature of the stick-slip behavior during the propagation of cracks usually seen in woven fabric composites. The stick-slip behavior is represented by the sudden failure of the fiber bridging during crack propagation [29]. The fiber bridging appears when the fibers act as crack arrestors that resist delamination, therefore, increasing the fracture toughness [30]. The presence of CNTs on the surface of the fibers tends to increase the maximum load value, which means that more energy is required for crack propagation. The fiber bridging of the samples is shown in Figure 8.

The Mode I interlaminar fracture toughness (G_{IC}) for woven fabric-reinforced laminated composite was calculated using CBT. G_{IC} of both the control sample (GF-Epoxy) and hybrid sample (CNTs-GF-Epoxy) as a function of crack growth are known as the *R*-curve. As shown in Figure 9, the interlaminar fracture toughness of hybrid sample demonstrated more unstable crack propagation compared to the control sample. The *R*-curve of hybrid sample tends to exhibit more stick-slip growth and higher fiber bridging than the control sample [31]. The sudden drop point of the *R*-curve during crack growth is due to the "run-arrest" behavior from the weave structure that forms a series of rapid propagation, followed by an arrest period [32]. The enhancement of the interlaminar fracture toughness was due to the presence of the CNTs deposited on the GF's surface improving the interlocking effect between the GF and epoxy matrix [33], improved delamination resistance of the fiber and fiber/matrix interface, and the increment of crack propagation [34].

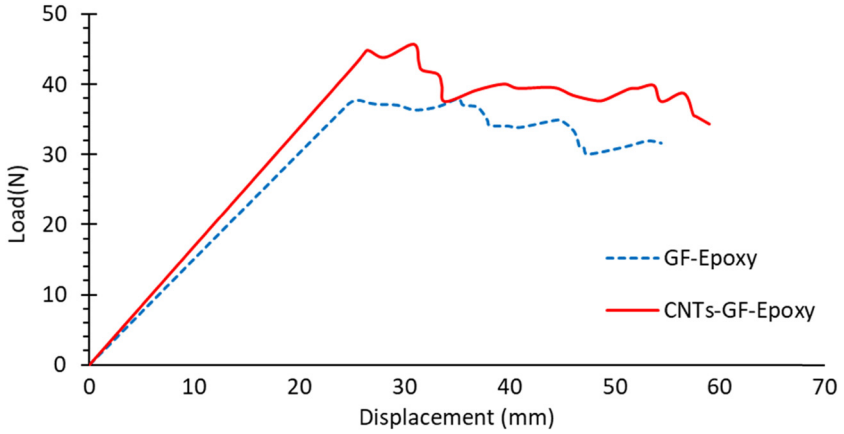

Figure 7: Load *versus* displacement curves for control sample (GF-Epoxy) and hybrid sample (CNTs-GF-Epoxy).

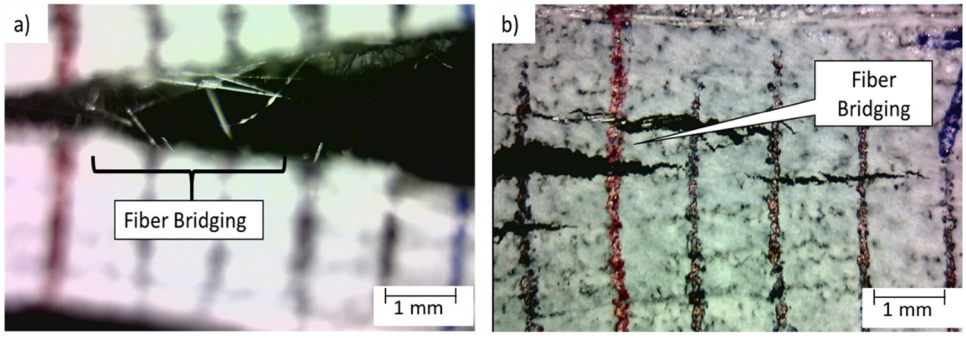

Figure 8: (a) and (b) Fiber bridging at DCB sample during crack propagation.

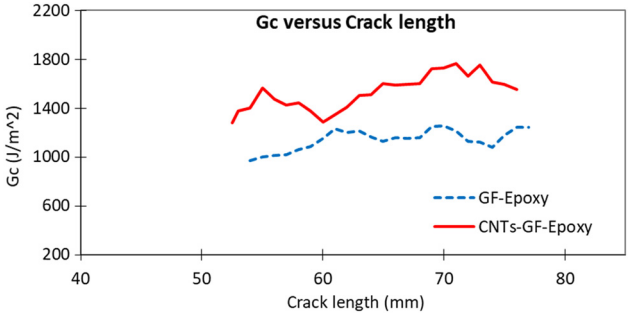

Figure 9: Mode I fracture toughness against crack length of control sample (GF-Epoxy) and hybrid sample (CNTs-GF-Epoxy).

Figure 10 shows the crack initiation of fracture toughness from the first point after a sudden decrease in the load, as indicated by the load *versus* displacement curves. The control sample GF-Epoxy has a crack initiation fracture toughness of 969.4 ± 17.3 J m^{-2}. The incorporation of CNTs into the composites improved crack initiation fracture toughness for the hybrid sample (CNTs-GF-Epoxy) by ~31.8% at 1277.5 J m^{-2}, which can be attributed to the increased interactions between the fiber and the matrix. The CNTs act as nano-bridges at the interfacial region, which increase energy absorption during crack propagations, thus enhancing the interfacial regions [35–37]. Compared to the control sample, the hybrid sample's propagation toughness increased by ~34.4% on average, where its G_{IC} was 1534.4 J m^{-2}. This improvement could be due to the fiber bridging phenomena, where fibers act as a crack arrestor, influencing the interlaminar fracture toughness as shown in Figure 8. Another toughening mechanism that simultaneously influences fracture toughness was crack-branching, polymer crazing, and fiber pull-out, as shown in Figure 12.

The flexural modulus of the arms from the DCB test were obtained using equation (7) as detailed in Section 2.4 and are tabulated in Figure 11. It was calculated as a function of the crack length. The flexural modulus of the hybrid sample was unaffected by the inclusion of the CNTs coated on the GFs. The control sample GF-Epoxy has a flexural modulus for the arm specimen of 10.60 ± 0.25 GPa, while the flexural modulus of the arm specimen for hybrid sample (CNT-GF-Epoxy) was 7.41 ± 0.22 GPa. The flexural modulus is independent of crack length [38].

The fracture behavior of the DCB samples of the GF-Epoxy and CNTs-GF-Epoxy were examined using FESEM at high magnifications, as shown in Figure 12. A clean fiber surface was observed at fractography of the control sample as shown in Figure 12a–c. There was clean separation between the fiber and matrix, which is indicative of adhesive failure and poor interfacial bonding.

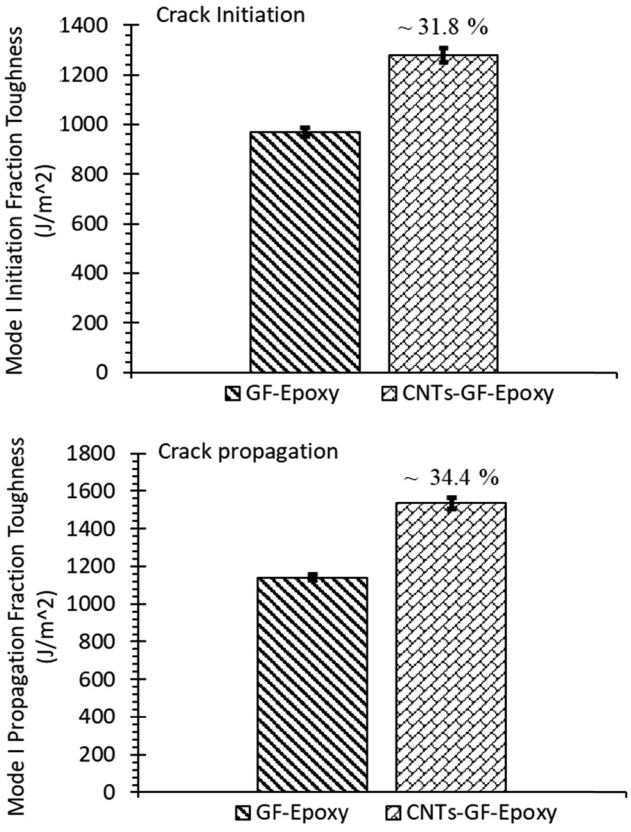

Figure 10: Comparison of the crack initiation and propagation fracture toughness for control sample (GF-Epoxy) and hybrid sample (CNTs-GF-Epoxy).

Detailed observation of interfacial debonding on fiber–matrix interphase is shown in Figure 12a–c. The incorporation of CNTs on the GF shows delamination, as per Figure 12d–h. The rough surface of the matrix fracture is seen mainly on the CNTs-GF-Epoxy in Figure 12e, which shows a more complicated fracture path, thus increasing fracture toughness. A hackles pattern within the fiber

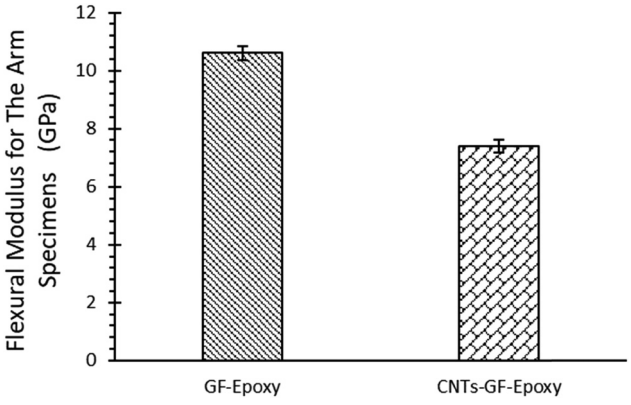

Figure 11: Comparison of flexural modulus for the arm DCB specimens.

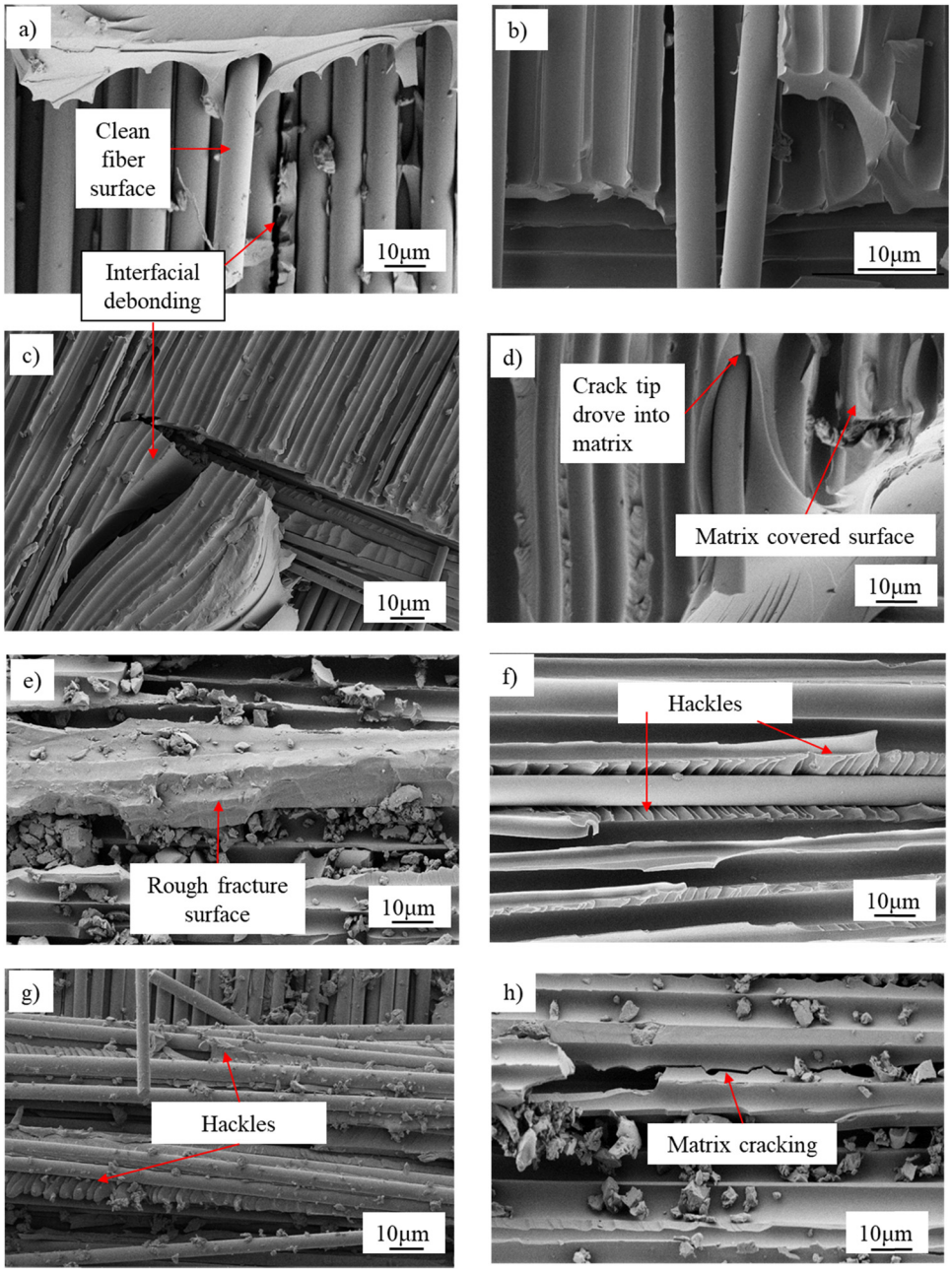

Figure 12: FESEM image of mode I fracture surface of the (a–c) control sample (GF-Epoxy); (d–h) hybrid sample (CNTs-GF-Epoxy).

side is shown in Figure 12f and g, developed at a high degree of deformation at the matrix phase by shear stress [39]. Additionally, Figure 12h shows the crack through the matrix, which indicated that the crack propagated cohesively within the matrix thus, promoting cohesive failure in the matrix. Consequently, at the end of the crack propagation, the hybrid sample with the presence of CNTs show significantly different mechanisms compared to the control sample (GF-Epoxy).

4 Conclusion

Hybrid CNTs-GF woven fabric material was manufactured using the ESD at an applied voltage of 18 kV and spray time of 30 min. A homogenous and uniform coating distribution of CNTs was found on the GF's surface using a high applied voltage. VARTM was used to fabricate the epoxy laminated composite. The interlaminar fracture toughness of the hybrid CNTs-GF-Epoxy increased by

~34% relative to its control counterpart. The presence of CNTs on GF improved the mechanical interlocking between the matrix and the fiber, hence increasing the cracking pathway leading to an increase in the interlaminar fracture toughness. This enhancement of fracture toughness was achieved on the hybrid sample where the CNTs were coated onto the fiber *via* the ESD method. Based on fractography observation on the interface, different failure mechanisms were found to have contributed to the interlaminar fracture toughness enhancement, thus confirming the (different) interactions between fiber and matrix due to the presence of the CNTs.

Funding information: The authors would like to acknowledge Universiti Sains Malaysia (USM) RUI 1001/PBAHAN/8014047 for sponsoring and providing financial assistant during this research work.

Author contributions: All authors have accepted responsibility for the entire content of this manuscript and approved its submission.

Conflict of interest: The authors state no conflict of interest.

References

[1] Fan Z, Santare MH, Advani SG. Interlaminar shear strength of glass fiber reinforced epoxy composites enhanced with multi-walled carbon nanotubes. Compos A Appl Sci Manuf. 2008;39(3):540–54.

[2] Mirjalili V, Ramachandramoorthy R, Hubert P. Enhancement of fracture toughness of carbon fiber laminated composites using multi wall carbon nanotubes. Carbon. 2014;79(1):413–23. doi: 10.1016/j.carbon.2014.07.084.

[3] Blake SP, Berube KA, Lopez-Anido RA. Interlaminar fracture toughness of woven E-glass fabric composites. J Composite Mater. 2012;46(13):1583–92.

[4] Wang B, Gao H. Fibre reinforced polymer composites. Cham: Springer; 2021. p. 15–43.

[5] Eskizeybek V, Avci A, Gülce A. The Mode I interlaminar fracture toughness of chemically carbon nanotube grafted glass fabric/epoxy multi-scale composite structures. Compos A. 2014;63:94–102.

[6] Shindo Y, Takeda T, Narita F, Saito N, Watanabe S, Sanada K. Delamination growth mechanisms in woven glass fiber reinforced polymer composites under Mode II fatigue loading at cryogenic temperatures. Compos Sci Technol. 2009;69(11–12):1904–11. doi: 10.1016/j.compscitech.2009.04.010.

[7] Nasuha N, Azmi AI, Tan CL. A review on mode-I interlaminar fracture toughness of fibre reinforced composites. J Physics Conf Ser. 2017;908(1):012024.

[8] Cui K, Zhang Y, Fu T, Wang J, Zhang X. Toughening mechanism of mullite matrix composites: a review. Coatings. 2020;10:7672.

[9] Aghamohammadi H, Eslami-Farsani R, Tcharkhtchi A. The effect of multi-walled carbon nanotubes on the mechanical behavior of basalt fibers metal laminates: an experimental study. Int J Adhes Adhesives. 2020;98:102538. doi: 10.1016/j.ijadhadh.2019.102538.

[10] Fanteria D, Lazzeri L, Panettieri E, Mariani U, Rigamonti M. Experimental characterization of the interlaminar fracture toughness of a woven and a unidirectional carbon/epoxy composite. Compos Sci Technol. 2017;142:20–9. doi: 10.1016/j.compscitech.2017.01.028.

[11] Shrivastava R, Singh KK. Interlaminar fracture toughness characterization of laminated composites: a review. Polym Rev. 2019;7(6):1020–45. doi: 10.1080/15583724.2019.1677708.

[12] Borowski E, Soliman E, Kandil UF, Taha MR. Interlaminar fracture toughness of CFRP laminates incorporating multi-walled carbon nanotubes. Polymers. 2015;7(6):1020–45.

[13] Barathi Dassan EG, Anjang Ab Rahman A, Abidin MSZ, Akil HM. Carbon nanotube-reinforced polymer composite for electromagnetic interference application: a review. Nanotechnol Rev. 2020;9(1):768–88.

[14] Chaudhry MS, Czekanski A, Zhu ZH. Characterization of carbon nanotube enhanced interlaminar fracture toughness of woven carbon fiber reinforced polymer composites. Int J Mech Sci. 2017;131–132:480–9.

[15] Khan SU, Kim J. Impact and delamination failure of multiscale carbon nanotube-fiber reinforced. Polym Composites: A Rev. 2011;12(2):115–33.

[16] Srivastava AK, Kumar D. Postbuckling behavior of functionally graded CNT-reinforced nanocomposite plate with interphase effect. Nonlinear Eng. 2019;8(1):496–512.

[17] Kośla K, Olejnik M, Olszewska K. Preparation and properties of composite materials containing graphene structures and their applicability in personal protective equipment: a review. Rev Adv Mater Sci. 2020;59(1):215–42.

[18] Kharissova VasilievnaO, Kharisov BI. In solubilization and dispersion of carbon nanotubes. Cham, Switzerland AG: Springer; 2017. p. 33–148.

[19] Hashim H, Salleh MS, Omar MZ. Homogenous dispersion and interfacial bonding of carbon nanotube reinforced with aluminum matrix composite: a review. Rev Adv Mater Sci. 2019;58(1):295–303.

[20] Zhang H, Kuwata M, Bilotti E, Peijs T. Integrated damage sensing in fibre-reinforced composites with extremely low carbon nanotube loadings. J Nanomaterials. 2015;2015(3):1–7.

[21] Zakaria MR, Akil HM, Omar MF, Abdullah MMAB, Rahman AAA, Othman MBH. Improving flexural and dielectric properties of carbon fiber epoxy composite laminates reinforced with carbon nanotubes interlayer using electrospray deposition. Nanotechnol Rev. 2020;9(1):1170–82.

[22] An Q, Rider AN, Thostenson ET. Hierarchical composite structures prepared by electrophoretic deposition of carbon nanotubes onto glass fibers. ACS Appl Mater Interfaces. 2013;5(6):2022–32.

[23] Demircan Ö, Çolak P, Kadıoğlu K, Günaydın E. Flexural properties of glass fiber/epoxy/MWCNT composites. Res Eng Struct Mater. 2019;5(2):91–8.

[24] Haghbin A, Liaghat G, Hadavinia H, Arabi AM, Pol MH. Enhancement of the electrical conductivity and interlaminar shear strength of CNT/GFRP hierarchical composite using

an electrophoretic deposition technique. Materials. 2017;10(10):1120.
[25] Rodriguez AJ, Guzman ME, Lim CS, Minaie B. Mechanical properties of carbon nanofiber/fiber-reinforced hierarchical polymer composites manufactured with multiscale-reinforcement fabrics. Carbon. 2011;49(3):937–48. doi: 10.1016/j.carbon.2010.10.057.
[26] Li Q, Church JS, Naebe M, Fox BL. A systematic investigation into a novel method for preparing carbon fibre–carbon nanotube hybrid structures. Compos A Appl Sci Manuf. 2016;90:174–85. doi: 10.1016/j.compositesa.2016.05.004.
[27] Zakaria MR, Md Akil H, Omar MF, Abdul Kudus MH, Mohd Sabri FNA, Abdullah MMAB. Enhancement of mechanical and thermal properties of carbon fiber epoxy composite laminates reinforced with carbon nanotubes interlayer using electrospray deposition. Compos C Open Access. 2020;3:100075.
[28] Vieille B, Casado VM, Bouvet C. About the impact behavior of woven-ply carbon fiber-reinforced thermoplastic- and thermosetting-composites: a comparative study. Compos Struct. 2013;101:9–21. doi: 10.1016/j.compstruct.2013.01.025.
[29] Mansour R. Mode I. Interlaminar fracture properties of oxide and non-oxide ceramic matrix composites [Internet]; 2017 [cited 2020 Nov 25]. Available from: http://rave.ohiolink.edu/etdc/view? acc_num=akron1494248628194216
[30] Khan R. Fiber bridging in composite laminates: a literature review. Compos Struct. 2019;229:111418.
[31] Pinto MA, Chalivendra VB, Kim YK, Lewis AF. Effect of surface treatment and Z-axis reinforcement on the interlaminar fracture of jute/epoxy laminated composites. Eng Fract Mech. 2013;114:104–14.
[32] Perrin F, Bureau MN, Denault J, Dickson JI. Mode I interlaminar crack propagation in continuous glass fiber/polypropylene composites: Temperature and molding condition dependence. Compos Sci Technol. 2003;63(5):597–607.
[33] Zhang H, Liu Y, Kuwata M, Bilotti E, Peijs T. Improved fracture toughness and integrated damage sensing capability by spray coated CNTs on carbon fibre prepreg. Compos A. 2015;70:102–10. doi: 10.1016/j.compositesa.2014.11.029.
[34] Warrier A, Godara A, Rochez O, Mezzo L, Luizi F, Gorbatikh L, et al. The effect of adding carbon nanotubes to glass/epoxy composites in the fibre sizing and/or the matrix. Compos A Appl Sci Manuf. 2010;41(4):532–8. doi: 10.1016/j.compositesa.2010.01.001.
[35] Tsantzalis S, Karapappas P, Vavouliotis A, Tsotra P, Kostopoulos V, Tanimoto T, et al. On the improvement of toughness of CFRPs with resin doped with CNF and PZT particles. Compos A Appl Sci Manuf. 2007;38(4):1159–62.
[36] Khosravi H, Eslami-Farsani R. Reinforcing effect of surface-modified multiwalled carbon nanotubes on flexural response of E-glass/epoxy isogrid-stiffened composite panels. Polym Compos. 2018;39:E677–86.
[37] Keshavarz R, Aghamohammadi H, Eslami-Farsani R. The effect of graphene nanoplatelets on the flexural properties of fiber metal laminates under marine environmental conditions. Int J Adhes Adhesives. 2020;103:102709. doi: 10.1016/j.ijadhadh.2020.102709.
[38] Blackman B, Kinloch A. Fracture tests on structural adhesive joints. European Structural Integrity Society. Kidlington, Oxford, UK: Elsevier; 2001. p. 225–67.
[39] Bonhomme J, Argüelles A, Viña J, Viña I. Fractography and failure mechanisms in static mode I and mode II delamination testing of unidirectional carbon reinforced composites. Polym Test. 2009;28(6):612–7.